A facile surface preservation strategy on the lithium anode for high performance Li-O_2 batteries

Zhihong Luo[2]‡, Guangbin Zhu[2]‡, Liankun Yin[2], Fujie Li[2], Ben Bin Xu[3], Laurent Dala[3], Xiaoteng Liu[3]*, Kun Luo[1,2]*

1. School of Materials Science and Engineering, Changzhou University, Changzhou 213164, P R China;

2. College of Materials Science and Engineering, Guilin University of Technology, Guilin 541004, P R China;

3. Department of Mechanical & Construction Engineering, Faculty of Engineering and Environment, Northumbria University, Newcastle upon Tyne, NE1 8ST, UK.

KEYWORDS: lithium metal anode; SiO_2/GO coating; protective layer; cyclic stability; Li-O_2 battery

ABSTRACT: Protecting anode from deterioration during charging/discharging has been seen as one of the key strategies in achieving high performance lithium (Li) -O_2 batteries and other Li metal batteries with high energy density. Here, we describe a facile approach to prevent the Li anode from dendritic growth and chemical corrosion by constructing a SiO_2/GO hybrid thin layer

on the surface. The uniform porous preserving layer can conduct Li ion in the stripping/plating process, lead to an effective alleviation of the dendritic growth of Li by guiding the ion flux through the microstructure. Such preservation technique significantly enhance the cell performance by enabling the Li-O_2 cell to cycle up to 348 times at 1 A·g^{-1} with a capacity of 1000 mAh·g^{-1}, which is several folds of the cycles of cells with the pristine Li (58 cycles), Li-GO (166 cycles) and Li-SiO_2 (187 cycles). Moreover, the rate performance is improved and the ultimate capacity of cell is dramatically increased from 5400 mAh·g^{-1} to 25200 mAh·g^{-1}. This facile technology is robust and conformal to the Li surface, which demonstrate the potential applications in developing future high performance and long lifespan Li batteries in a cost-effective fashion.

INTRODUCTION

Aprotic Li-O_2 battery (LOB), a promising energy solution for automotive and aerospace engineering, has superior advantage in its high energy densities, when comparing with conventional lithium/sodium ion batteries (LIB/SIB).[1-8] Currently, the technical development in aprotic LOBs encounters substantial bottlenecks, including high charge overpotential, passivation of cathode, poor stability of electrolyte and Li metal anode.[7] Significant efforts have been devoted to enhancing the cyclic stability and other electrochemical performance of LOBs, by promoting the sluggish kinetics of oxygen reduction and evolution with using proper catalysts,[9] porous cathode materials,[10,11] redox mediators[12,13] and stable electrolytes.[14,15]

Despite its natural scarcity, problematic stability and safety issues,[7,8] Li metal is regarded as an ideal anode material for rechargeable batteries due to its super high specific energy (3860 mAh·g^{-1}), low redox potential (-3.04 V vs. SHE) and low mass density (0.534 g·cm^{-3}). However,

Li anodes encounter challenges such as the uneven stripping/plating of Li ions and the low Coulombic efficiency during charge/discharge cycles, which usually lead to the dendritic growth of Li to cause the short-circuiting and "dead Li" (i.e. broken Li branches) after repeated charging/discharging operation,[16] and a rapid degradation in battery cell.[17] The decaying in LOBs can be accelerated as the crossover oxidative species like soluble oxygen reduction intermediates (O_2^- and LiO_2^- etc.), H_2O and other reaction by-products can accelerate Li loss, thus result in a declined cycle life.[18,19]

One of the recent research interests has been focused on the protection of Li anodes, since the dendritic deposition of lithium metal and dendrites formation along solid-electrolyte interphase (SEI) are unveiled as key issues to determine the safety and performance for LOBs.[20,21] The exercised strategies for protecting Li anodes can be categorized in the following: (1) Using poreless, air-impermeable and waterproof separators, to prevent O_2, H_2O and other soluble species in the electrolyte from corroding anode in LOBs,[22-24] however, the increase of the overall cell resistance remains under concerning. (2) Optimizing the structure of SEI layers, where the lifespans of LOBs can be extended after treating the SEI layers on Li anodes chemically (including reaction with CO_2, N_2 and F, B containing electrolyte additives)[25-29] or electrochemically.[30-32] (3) Generating ionically conductive, mechanically robust and chemically stable protection layer(s) on Li anodes, and the commonly used materials for such protection layer includes, polymers (e.g. poly(1,4-dioxacyclohexane)[33]), inorganic compounds (e.g. germanium or indium compounds[34-36]) and composites (e.g. Al_2O_3/PVDF-HFP or AlF_3/PEDOT -PEG[37,38]) layers.

Graphene and graphene oxide (GO) have been reported previously to offer protection to Li anode by preventing from dendrite growth, corrosion and strengthening the stability of SEI[39-43]. Li and co-workers[39] employed reduced graphene oxide to prevent Li dendrite through directing its

growth. Zhao et. al. [41] encapsulated Li alloy with graphene sheets to prevent the corrosion from air. Gao and co-workers[43]designed a molecular-level SEI by embedding polymeric Li salts with graphene oxide, which provides the SEI to have excellent stability and good passivation properties, that prevents the Li metal anode from dendrite growth and corrosion. Silica were also used for Li metal protection. Tang and co-workers applied silica nanoparticles in cross-linked polymer solid-state electrolyte for increasing Li ionic conductivity by forming 3D ion transport paths.[44] Lin et. al. employed silica aerogel as backbone for a polymer electrolyte for high Li ionic conductivity and modulus.[45] Herein, we propose an anode protection strategy by developing an artificial composite layer consisting of silica nanoparticles (SiO_2 NPs) and GO nanosheets, on the Li metal (Li-SiO_2/GO) anode. GO sheets serve as a barrier to hinder the growth of Li dendrites and the deteriorative attack of oxygen species from electrolyte, the SiO_2 NPs embedded in GO sheets can provide effective interlayer and pores for Li ions diffusion by preventing the aggregation of GO sheets. With this designed protection, the LOBs with Li-SiO_2/GO anodes exhibit superior cyclic stability, rate performance and ultimate capacity. We hope this anode protection technology will find future applications in next generation sustainable energy solutions.

EXPERIMENTAL

Chemicals and materials. Potassium permanganate ($KMnO_4$, AR, Sinopharm Group), hydrogen peroxide (H_2O_2, 30%, Sinopharm Group), sodium nitrate ($NaNO_3$, AR, Sinopharm Group) and sulphuric acid (H_2SO_4, AR, Sinopharm Group) were used as received. Dimethyl ether (DME, anhydrous, 99.5%, Sigma-Aldrich), dimethyl sulfoxide (DMSO, 99.9%, Sigma-Aldrich) and propylene carbonate (PC, 99.7%, Sigma-Aldrich) were dehydrated with activated 4 Å molecular sieves. Lithium perchlorate ($LiClO_4$, 99.99%, Sigma-Aldrich) was dried at 160 ºC in a vacuum oven for 12 h prior to use. Graphite (Sigma-Aldrich), silica NPs (SiO_2, d = 30 ± 5 nm,

Shanghai Keyan Co. Ltd.), multi-walled carbon nanotubes (MWNTs, d = 10 ± 1 nm, L = 3 ~ 6 μm, Sigma-Aldrich), carbon paper (TORAY, TGPH-060) and borosilicate glass fibre (GF, d = 18 mm, Whatman) were used as received. Li plates (d = 14 mm, Shenzhen Poxon Machinery Technology Co. Ltd.) were saturated in a PC solution containing 0.1 M $LiClO_4$ for at least 48 h before use.

Preparation of SiO_2/GO hybrids. GO was prepared using the modified Hummer's method.[46] Typically, 1.0 g graphite, 0.5 g $NaNO_3$ and 23 mL H_2SO_4 were mixed and stirred at 0 °C for 1 h. The mixture was heated to 35 °C, then 3.0 g $KMnO_4$ was slowly added. After stirring for 7 h, another 3.0 g $KMnO_4$ was added and the mixture was kept stirring for next 12 h. The mixture was cooled down in air and then 400 mL of ice water were added under stirring. After that, 30 wt% H_2O_2 was gradually added till the color of mixture turned from brown to yellow. The solid content in mixture was separated by centrifugation at 8000 rpm, then repeatedly rinsed with deionized water till the supernate became neutral. The precipitate was mixed with deionized water under ultrasonic stirring for 3 h, and then allowed to stand for 12 h. The GO suspension in the container was removed and used for further synthesis.

SiO_2 NPs were ultrasonically dispersed in the GO suspension with a mass ratio of 1:2 (SiO_2/GO) for 2 h, the precipitate was then removed and dried in a vacuum oven at 80 °C for 24 h. The dried SiO_2/GO powder was carefully ground, then dispersed into DME (5 mg·mL^{-1}), where 0.5 mg of the slurry were repeatedly pipetted until formed a full coverage on the surface of a Li plate followed by smoothen process using a fine blade, after drying in glove box at ambient temperature the Li anode with protective SiO_2/GO coating is obtained and marked as Li-SiO_2/GO. The Li anodes coated with either mono-component SiO_2 or GO were prepared as reference samples, denoted as Li-SiO_2 and Li-GO, respectively. Various GO/SiO_2 mass ratios (0.5:1, 1:1, 2:1, 3:1 and

4:1) and loading amounts (0.1 mg, 0.2 mg, 0.6 mg, 0.8 mg, 1.0 mg and 1.5 mg) were prepared and constructed as preserving layer on the Li anodes.

Battery assembly and testing. The batteries were assembled and built into CR2032 coin cells in an Ar-filled glove box (MIKROUNA, Super, H_2O < 0.1 ppm, O_2 < 0.1 ppm), and tested by a standard battery testing system (CT-3008W-5V10mA, Neware Technology Limited).

LOBs were assembled using both Li anodes and MWNTs cathodes in the CR2032 cells. The Li anodes employed in the experiment included the pristine Li plate and Li plates with different surface coatings. The cathode was prepared by spraying the MWNTs in ethanol slurry onto carbon paper at a loading of 0.1 $mg{\cdot}cm^{-2}$. To assemble the coin cells, an anode cap was firstly placed, and then a Li anode (either the pristine Li or one of the anodes with surface coatings), a glassy fiber separator (wetted with 100 μL of 1 M $LiClO_4$/DMSO electrolyte), a MWNTs cathode and a cathode cap were placed in a sequence and encapsulated. The cells were mounted separately in the holders of a home-made battery testing box filled with pure oxygen at 1.0 atm. The cyclic performance test was settled at a rate of 1 $A{\cdot}g^{-1}$ with a fixed capacity of 1000 $mAh{\cdot}g^{-1}$ within the potential window from 2.0 V to 4.5 V. The rate performance was measured at the current densities of 2 $A{\cdot}g^{-1}$, 3 $A{\cdot}g^{-1}$ and 5 $A{\cdot}g^{-1}$ and the capacity of 1000 $mAh{\cdot}g^{-1}$ within the potential cut-offs from 2.0 V to 4.5 V.

To characterize the ionic conductivity of coating layers, Li|SS (stainless steel) cells were assembled and subjected to the analysis of electrochemical impedance spectroscopy (EIS) in O_2 free atmosphere. An anode cap, a Li plate, a glass fiber separator (wetted with 100 μL of 1 M $LiClO_4$/DMSO electrolyte), a SS plate and CR2032 cathode cap (without holes) were placed in sequence and encapsulated to construct a Li|SS cell. To investigate the stability of Li anodes with

surface coatings in O_2 atmosphere, Li|SS foam cell were assembled, the approach is similar to Li|SS cell except using CR2032 cathode cap with holes and SS foam to replace SS plate. The Li|SS cells and Li|SS foam cells with Li-GO, Li-SiO_2 and Li-SiO_2/GO were also assembled with the same approaches. To characterize the resistance of LOBs (the assembly approach was the same to LOBs) after cycling for certain times, the EIS test was carried out after introducing N_2 to remove any O_2. All EIS plots were recorded on an electrochemical station (CHI 660, CH Instrument) at an open circuit potential with 5 mV of ac amplitude in the frequency range from 0.1 Hz to 1 MHz.

Symmetric Li|Li cells were assembled to investigate the protection of Li anodes with different coatings in O_2 free atmosphere, where an anode cap, a Li plate, a glassy fiber separator (wetted with 100 μL of 1 M $LiClO_4$/DMSO electrolyte), another Li plate and CR2032 cathode cap (without holes) were placed in sequence and encapsulated. In the case with O_2, Li plate with a hole (diameter of 2 mm) and CR2032 cathode cap with holes were used, the assembly approach was similar to those without O_2. The same approach was also applied to the assembling of symmetric Li|Li cells with Li-GO, Li-SiO_2 and Li-SiO_2/GO. The charge/discharge cycling was carried out with a time period fixed for 1 h at the current density of 0.1 $mA{\cdot}cm^{-2}$.

Characterization. A field-emission scanning electron microscope (SEM, S-4800, Hitach) and a transmitting electron microscope (TEM, JEM-2100F) operating at 200 kV were employed to observe the morphology of the anodes and cathodes. X-Ray diffractometer (XRD, X'Pert PRO) equipped with Cu Kα radiation (λ = 1.54059 Å) was used to characterize the composition and structure of the coating and battery discharge products. X-ray photoelectron spectroscope (XPS, ESCALAB 250Xi, Thermo Fisher Scientific) using Al kα radiation was applied to characterize the component of coating layers and SEI. The electron conductivity of coating layers was measured by High Temperature Resistivity Measurement System (RMS-1000I, Partulab Techologies). The

specific surface area was measured by the N_2 adsorption/desorption isotherms by a surface area analyser (NOVA1200e, Quantachrome).

RESULTS AND DISCUSSION

Structural identification of protective coating layers. Figure 1a reveals a laminated structure for the SiO_2/GO coating layer, i.e. the SiO_2 NPs are intercalated among GO sheets, which effectively inhibit the overlap aggregation of GO sheets and thereby produces nano/mesopores for Li ions transportation. Two more cells with SiO_2 and GO individually coated anode were also assembled and tested for comparison purpose, this is to reveal the combined functions from both SiO_2 and GO when they are laminated together. Morphology information of SiO_2 and GO are shown in TEM images in Figure. S1.

The N_2 adsorption/desorption isotherms in Figure 1b demonstrate that both the SiO_2 and SiO_2/GO exhibit the type IV nitrogen sorption isotherms, while the GO presents a low porosity likely due to the re-stack of the GO sheets. Based on the Brunauer-Emmett-Teller (BET) method, the SiO_2/GO coating delivers a specific surface area of up to 172.70 $m^2 \cdot g^{-1}$, and the SiO_2 presents a specific surface area of 146.25 $m^2 \cdot g^{-1}$, and the specific surface area of the GO is just 2.35 $m^2 \cdot g^{-1}$. The estimated average pore sizes are 5.42 nm with a pore volume of 1.9×10^{-3} $cm^3 \cdot g^{-1}$ for the GO layer, 6.27 nm with a pore volume of 176×10^{-3} $cm^3 \cdot g^{-1}$ for the SiO_2 layer, 3.8 nm with the largest pore volume of 312×10^{-3} $cm^3 \cdot g^{-1}$ for the SiO_2/GO layer (Figure 1c). The largest specific surface area of SiO_2/GO coating layer is caused by the intercalation of SiO_2 NPs among the GO sheets, this is in good agreement with the TEM result in Figure 1a.

Next, we use XRD to assess the structure for coating layers (Figure 1d). For the GO coating, an intense and sharp peak is observed at 8.8° corresponding to the interplanar spacing of ca. 1.0

nm of GO sheets,[47] and a bump at 25.2° resulted from the oxidized graphite. The XRD pattern of SiO_2 presents a broad peak at 22.6°, assigned to the (101) facet of silica (JCPDF 82-1235). As for the SiO_2/GO hybrid, a broad peak appears at about 22.6°, possibly attributed to the overlapped oxidized graphite and SiO_2 peaks, and the diffraction of the GO at ca. 8.8° is vanished which indicates no GO aggregation, in line with the TEM and BET analyses. We further applied XPS to characterize the component of coating layers (Figure S2). C_{1s} spectrum of GO layer shows four peaks at 284.8, 286.5, 287.6, 290.0 eV, which are assigned to C-C, C-OH, C=O and COOH groups, respectively (Figure S2a). Si_{2p} of SiO_2 layer spectrum displays one peak at 103.5 eV attributed to SiO_2 (Figure S2b). C_{1s} and Si_{2p} spectra of SiO_2/GO layer exhibit similar peaks, indicating that SiO_2 /GO composite contains the same component of GO and SiO_2 (Figures S2c, S2d).

SEM images of pure Li and Li-GO, Li-SiO_2, and Li-SiO_2/GO are showed in Figures 1e-l. For the pristine Li (Figure 1e), a flat and smooth surface is observed with a uniform SEI layer on top of Li plate (Figure 1i). However, the SEM image for Li-GO (Figures 1f, 1j) and Li-SiO_2 (Figures 1g, 1k) indicate rough/loosen surfaces.[48] For the Li surface coated with SiO_2/GO hybrid (Figures 1h, 1l), a smooth and compact surface layer was obtained, where the composite layer shows a good adhesion to the Li surface. The protective layers are marked with orange color dash line, which are 20.5, 24.5 and 22.0 μm for GO, SiO_2 and SiO_2/GO layer, respectively. The electron conductivity of GO, SiO_2 and SiO_2/GO composites is tested, which is 3.03×10^{-6}, 5.59×10^{-8}, and 1.09×10^{-6} $S\cdot cm^{-1}$(Figure 2d), respectively.

Standard EIS analysis is used to compare the effect of GO, SiO_2 and SiO_2/GO coatings on the Li ion conductivity in the Li|SS cells versus the pristine Li, which is listed in Figure 2c.[38] The Nyquist plot (Figures 2a, 2b) shows the intercept of real axis represents the impedance of Li^+ diffusion (R_s) from the electrolyte solution to lithium metal.[38,49] In the cell with pristine Li, the

impedance is 3.01 Ω. Comparing to pristine Li, the impedance of the GO layer is 34.39 Ω, representing with the Li ion conductivity of 1.56×10^{-4} S·cm^{-1}, this increase is due to the re-stack of GO sheets that hinders the Li ion diffusion in line with previous reports.[47,50] Li-SiO_2 delivers a comparable impedance of 3.21 Ω to pristine Li, indicates the high Li ion conductance (2.01×10^{-3} S·cm^{-1}) within SiO_2 NPs layer. The Li-SiO_2/GO exhibits a resistance of 7.76 Ω (conductivity of 7.46×10^{-4} S·cm^{-1}) for Li ion diffusion, which resulted from the high porosity of the hybrid layer that enhances the Li ion conductivity. EIS analysis with Li|SS foam cells are conducted in O_2 atmosphere to compare the stability of Li anodes with or without coating layers. As displayed in Figure S3a, the Nyquist plot of pristine Li anode are varied after staying in O_2 atmosphere for 2 days, in contrast, with GO, SiO_2 and SiO_2/GO coatings (Figures S3b-d), the Nyquist plots for cells after two days showed slight variation, implying the stability of Li anodes with coating layers have been improved.

Li Symmetric Battery performance evaluation. We carried out the galvanostatic charge/discharge measurement to investigate the impact of surface coatings on the long-term cyclic stability of Li symmetric battery with GO, SiO_2 and SiO_2/GO coating layers. The Li|Li cells with a pair of pristine Li electrodes can only cycle for 134 h (Figure 3a), whereas a longer lifetime of 412 h is achieved after coating GO on the Li electrodes. The cycle life is further extended to 1200 h and 1000 h, respectively, by using the SiO_2 and SiO_2/GO coatings. The cycling performance of Li, Li-GO, Li-SiO_2 and Li-SiO_2/GO electrodes are compared within the initial 4 h (Figure 3b), where the Li, Li-SiO_2 and Li-SiO_2/GO exhibit similar voltage profiles during the Li stripping/plating process at the magnitudes of about 26 mV. However, the Li-GO presents a larger value of 48 mV, suggesting that a higher resistance was generated by the GO coating. From 132 h to 136 h (Figure 3c), the voltage oscillation of Li-GO increased to ca. 70 mV, and the values of

Li-SiO_2 and Li-SiO_2/GO electrodes remain unchanged. The pristine Li presents a sharp increase of overpotential after 135 h, suggesting a battery failure.[51] In Figure 3d, the voltage hysteresis of Li-GO is noticeably broadened over 600 mV between 408 h to 412 h, indicating a battery failure; however, the amplitudes of the Li-SiO_2 and Li-SiO_2/GO maintain stable below 24 mV. After 614 h (Figure 3e), the potential oscillation of Li-SiO_2/GO (88 mV) becomes larger than the Li-SiO_2 (34 mV), and keeps increasing to 475 mV till the battery fails at 1000 h. The Li-SiO_2 manifests the longest cycling life and end up at 1200 h.

The morphology of Li metals during cycling were characterized and showed in Figures 3f-m. After 200 h operation, Li metal of Li|Li cell exhibits coarse surface topped with mossy Li (Figure 3f, top view SEM image), and side view SEM image shows large cracks appeared on the top layer, with several cracks showed clear tendency of development to deeper layers (Figure 3j). With GO coating only, from top view image (Figure 3g), cracks caused by mossy Li are still observed on the surface of Li metal, however, cracks are hardly seen on the side view image (Figure 3k). Both Figure 3j and 3k show fluffy profile on top layer mossy Li which looks different to pure Li metal, this is the evidence that surface of these two anodes has been corroded. Those cells with SiO_2 (Figures 3h and 3l) and SiO_2/GO (Figures 3i and 3m) coating layers, have no obvious mossy Li and cracks can be seen after cycling for 800 h, in addition the cross-sectional image shows compacted SEI. These results demonstrate that SiO_2 and SiO_2/GO coating layers can facilitate stable SEI formation and regulate Li deposition.

The long-term cyclic stability of Li symmetric battery with GO, SiO_2 and SiO_2/GO coating layers were also investigated in O_2 atmosphere. As shown in Figure S4a, the Li|Li cells with pristine Li electrode can only cycle for 80 h, in contrast, the cells with GO, SiO_2 and SiO_2/GO layer can cycle up to 250, 300 and 480 h, respectively. During the first 4h (Figure S4b), Li|Li cells

with pristine Li, Li-SiO_2 and Li-SiO_2/GO present discharge overpotential of 8 mV, but it is 34 mV for Li-GO electrode. In charge process, Li|Li cells with pristine Li, Li-GO and Li-SiO_2 shows overpotential of 36 mV, and 16 mV for Li-SiO_2/GO electrode. The Li|Li cell with Li-SiO_2/GO electrode also exhibits the smallest overpotential during discharge and charge process. This could because SiO_2/GO layer formed the most stable SEI on Li surface. From 80 h to 84 h (Figure S4c), Li|Li cell with pristine Li shows potential oscillation severely, this is an indication of the cell failure. However, Li|Li cells with Li-SiO_2 and Li-SiO_2/GO electrode showed overpotential of 44 mV, but Li-GO electrode showed 72 mV. After 250 h (Figure S4d), the overpotential of Li|Li cells with Li-GO Li-SiO_2 electrodes increased 2 V and 700 mV, respectively, but the increase is only about 100 mV for the cell with Li-SiO_2/GO electrode. After 300 h (Figure S4e), the increase in overpotential of Li|Li cells with Li-SiO_2 electrode is more than 2 V, but it is only 140 mV for the one with Li-SiO_2/GO electrode. Although the overpotential increases during the Li stripping/plating process in O_2 atmosphere, the cell with Li-SiO_2/GO electrode still maintains the lowest overpotential, implying the SiO_2/GO layer improves the stability of Li anode.

The morphology of Li electrodes from Li|Li cells cycling in O_2 atmosphere can be found in Figures S4f-m. After cycling for 80 h, Li electrode generated lots of powders on the surface (Figure S4f), large cracks and a thick layer of powders from the side view can be observed (Figure S4j), this white powder is the corrosion products of LiOH. Morphology of Li-GO, Li-SiO_2 and Li-SiO_2/GO electrode after operating for 200 h are also characterized. Compared to Li electrode, Li-GO and Li-SiO_2 anode produced less powder on the surface (Figures S4g, h) and no obvious cracks from side view (Figures S4k, l). Li-SiO_2/GO electrode shows appearance with smoother surface and better evenly distributed cross-section (Figures S4i, m).

Li-O_2 Battery performance evaluation. The cyclic stability and rate performance of the LOBs with the pristine Li, Li-GO, Li-SiO_2 and Li-SiO_2/GO anodes are assessed and compared (Figure 4). The cell with pristine Li can only operate for 58 cycles (Figure 4a). The discharge potential stays at about 2.72 V before the 15th cycle, and then gradually dropped to 2.22 V at the 58th cycle. The charge potential keeps increasing from 4.10 V from the 1st cycle and ends up with ca. 4.24 V at the 58th cycle. The charge/discharge profiles of the cell with Li-GO anode in Figure 4b, suggest a better cyclic performance for 166 times. The discharge plateau maintains at 2.79 V within the initial 58 cycles, which then reduced down to 2.63 V at the 166th cycle. The charge plateau starts from 3.90 V at the 1st cycle and gradually increases to 4.42 V at 166th cycle. The cell with Li-SiO_2 anode can cycle for 187 times as displayed in Figure 4c, during which the discharge voltage maintains at 2.76 V within 120th cycles, and finally decreases to 2.64 V at the 187th cycle. The charge voltage locates at 3.83 V at the 1st cycle and approaches to 4.41 V at the end.

Interestingly, the Li-SiO_2/GO anode (Figure 4d) presents the best battery performance with significantly extended lifespan of LOB cell to 348 times. The discharge voltage remains above 2.70 V for 230 cycles, then declines to 2.43 V at the 348th cycle. The charge voltage begins with just 3.03 V at the 1st cycle, which increases to 3.68 V at the 58th cycle, 3.98 V at the 230th cycle, 4.12 V at the 290th cycle, and finishes as 4.30 V at the 348th cycle. The LOB with the Li-SiO_2/GO anode also renders better rate performance than the others (Figures 4e-h). At rate of 2 A·g^{-1}, the cell with the Li-SiO_2/GO anode can operate for 194 times, higher than the cells with the pristine Li (46 times), Li-GO (116 times) and Li-SiO_2 anodes (118 times). At the rate of 3 A g^{-1}, the cells with the pristine Li, Li-GO and Li-SiO_2 anodes can run for 34, 53 and 59 cycles, and the cell with the Li-SiO_2/GO anode can run for 83 times. At 5 A·g^{-1}, the cells with the pristine Li, Li-GO and

Li-SiO_2 anodes can cycle for 26, 33 and 36 times, and the cell with the Li-SiO_2/GO anode can operate for 56 times. Moreover, an ultimate capacity of the LOB with Li-SiO_2/GO anode is achieved at 25200 $mAh \cdot g^{-1}$ (Figure S5), while the cells with pristine Li, Li-GO and Li-SiO_2 anodes show values as 5400 $mAh \cdot g^{-1}$, 19900 $mAh \cdot g^{-1}$ and 23700 $mAh \cdot g^{-1}$, respectively.

The LOB performance can be affected by the SiO_2/GO mass ratio and loading amount. As shown in Figure S6a, the cycle numbers of the Li anodes with SiO_2/GO coatings are larger than those with sole GO or SiO_2 coating, the best performance appears at the SiO_2/GO mass ratio of 1/2. In Figure S6b, we obtain the cycle numbers of 160, 180, 348, 215, 192, 176 and 159, for the Li-SiO_2/GO anodes with a SiO_2/GO weight of 0.1 mg, 0.2 mg, 0.5 mg, 0.6 mg, 0.8 mg, 1.0 mg and 1.5 mg, respectively, with the SiO_2/GO mass ratio of 1/2. An optimized loading is determined to be 0.5 mg of the coating materials applied on Li anode. The TEM images of SiO_2/GO with different mass ratio demonstrate that SiO_2 nanoparticles severely aggregate when GO/SiO_2 ratio is 0.5/1 (Figure S7a) and 1/1 (Figure S7b), and no SiO_2 nanoparticles fills in some area of GO layers, multi-layer covers of GO are also observed when the GO/SiO_2 ratio is 3/1(Figure S7c) and 4/1(Figure S7d). The side view SEM images of the Li-SiO_2/GO with different loading amounts (Figure S8) reveal a smooth and compact morphology for the SiO_2/GO layers when the loading amount is less than 0.6 mg, and a rough and cracked morphology when the loading mass exceeds 1.0 mg, which is in agreement with the above battery testing results.

Structural examination and failure analysis for variant Li anodes after cycling. SEI evolution of Li anodes is investigated by XPS (Figure 5, Table S1). For pristine Li anode (Figure 5a, top 3 spectra), C_{1s} spectrum shows three peaks at 284.8, 286.8 and 288.8 eV, Li_{1s} spectrum exhibits a peak at 55.4 eV, and O_{1s} spectrum displays two peaks at 531.7 eV and 533.1 eV, these indicate the existence of RCOCOOLi after soaking in PC electrolyte for 48 h. As for Li-GO (Figure

5b, top 3 spectra), Li-SiO_2 (Figure 5c, top 3 spectra), and Li-SiO_2/GO anodes (Figure 5d, top 3 spectra), C_{1s} spectrums exhibit three peaks at 284.8, 285.5 and 288.8 eV, Li_{1s} shows a peak at 55.4 eV and O1s shows a peak at 532.6 eV, attributing to the RCH_2COOLi. The discrepancies between the Li anodes with or without coating layers possibly because that Li plates with coating layers aren't pretreated with PC electrolyte, and DME used as dispersant for GO and SiO_2 composites contributed to the formation of RCH_2COOLi. After cycling for 10 times, the C_{1s} spectra of Li (Figure 5a, bottom 3 spectra), Li-GO (Figure 5b, bottom 3 spectra) and Li-SiO_2 (Figure 5c, bottom 3 spectra) anodes show three peaks at 284.8, 285.5 and 288.8 eV, Li_{1s} spectra display two peaks at 54.6 and 55.4 eV, and O_{1s} spectra exhibit two peaks at 531.2 and 532.6, Li_{1s} of 54.6 eV and O_{1s} of 531.2 eV belong to LiOH, indicating that the corrosion of Li anode occurs. In contrast, for Li-SiO_2/GO anode (Figure 5d, bottom), C_{1s} spectrum shows four peaks at 284.8, 285.4, 288.8 and 289.9 eV, Li_{1s} and O_{1s} exhibits one peaks at 55.4 and 532.6 eV, respectively. C_{1s} of 289.9 eV assigns to Li_2CO_3, possibly because the oxygen-groups of GO participate to the formation of SEI. These results imply that after 10 cycles RCOOLi and Li_2CO_3 are the main component of SEI, corrosion of Li-SiO_2/GO anode by H_2O is inhibited by the SiO_2/GO coating layer.

Morphological evolution after charge/discharge cycling reveals the role of surface coating on preserving the Li anode. Figure 6a show the pristine Li and the pulverized anode after 58 cycles, which originally possesses a thickness of 348 μm (Figure 6e), suggesting that the battery failure is associated with the fast consumption of Li. The Li-GO anode presents a rough surface at the 58^{th} cycle (Figure 6b), where Li metal still remains in a thickness of 172 μm (Figure 6f). The Li-SiO_2 anode also shows coarsen and scraggy surface after cycling for 58 times (Figure 6c), leaving Li metal in a thickness of about 186 μm (Figure 6g). As for the Li-SiO_2/GO anode, a smooth and compact surface is retained after 58 cycles (Figure 6d) with the average thickness of metallic Li

for up to 264 μm (Figure 6h), which offers a solid evidence to show the effective protection by the SiO_2/GO hybrid coating. Figures 6i, 6j, 6k and 6l display the XRD patterns of powder from Li, Li-GO, Li-SiO_2 and Li-SiO_2/GO anodes' surface after 58 cycles. The powders from the pristine Li anode manifest eleven peaks at 20.4°, 32.5°, 35.7°, 41.6°, 49.2°, 51.4°, 56.0°, 62.2°, 73.9°, 75.7° and 79.4°, which can be assigned to the (001), (101), (110), (002), (102), (200), (112), (211), (212), (220) and (221) facets of LiOH crystal (JPDF No. 85-0736). The intensity decreases in the order of pristine Li, Li-GO, Li-SiO_2 and Li-SiO_2/GO anodes, indicating the decreased amount of LiOH, in-line with the increase thickness of Li anode after 58 cycles (Figures 6f-h). This further proved corrosion of Li anode has been alleviated by the protective coating. The SEM images and XRD patterns of Li-GO anodes after 166 cycles (Figures S9a, S9d), Li-SiO_2 anodes after 187 cycles (Figures S9b, S9e) and Li-SiO_2/GO anodes after 348 cycles (Figures S9c, S9f) exhibit the same feature as the pristine Li anode, which indicate the identical products at battery failure.

It has been reported that highly active cross-over oxygen reduction intermediates (O_2^- and LiO_2^- etc.) attack Li anode and cause corrosion, they also react with electrolyte and produce water molecules which is harmful to Li metal.[15,18,23,31] Sun et al., revealed the side reaction and volume evolution of Li anode also damage the cathode using Neutron Tomography.[52] Our previous work indicates that the protection of Li anode by creating stable SEI can also alleviate the passivation of cathode.[31] Here, Figure 7 shows that when Li anode is protected with artificial layer, such as GO, SiO_2 and SiO_2/GO, the accumulation of the solid products on cathode is reduced.

Accumulation of solid discharge products can result in the passivation of MWNTs cathode, thus lead to battery failure, which can be traced from the SEM image of the pristine MWNTs cathode in Figure 7a. For the cell with a pristine Li anode (Figure 7b), the MWNTs cathode is totally covered with large blocks of discharge products at the 58^{th} cycle, represent a passivation of

battery cathode. As for the cells with the Li-GO (Figure 7c), Li-SiO_2 (Figure 7d) and Li-SiO_2/GO (Figure 7e) anodes, bare MWNTs can still be observed after 58 cycles, where the amount and particle size of the deposit in the cell with the Li-SiO_2/GO anode are apparently less than the others. The MWNTs cathodes are finally cladded by large deposit blocks for the cells with the Li-GO (Figure 7f), Li-SiO_2 (Figure 7g) and Li-SiO_2/GO (Figure 7h) anodes after 166, 187 and 348 cycles, respectively, illustrating the alleviation of discharge product accumulation with the application of protective coatings on the Li anodes.

XRD analysis indicates that the MWNTs cathode in the cell with the pristine Li anode after 58 cycles manifests two peaks at 26.4° and 54.5°, corresponding to the (002) and (004) facets of MWNTs (JPDF No.41-1487) as shown in Figure S10a, and the peak at 32.5° can be attributed to the (101) facet of LiOH crystal (JPDF No.85-0736). In correspondence, the MWNTs cathode in the cell with the Li-SiO_2/GO anode also presents one peak in at 32.5° attributed to the (101) facet of LiOH (JPDF No. 85-0736) at the 58^{th} cycle (Figure S10b), and the intensity is much lower than that of the cell with pure Li, indicating less solid products accumulated, this is confirmed in SEM image of cathode (Figure 7e). At the 348^{th} cycle (Figure S10c), the intensity of the three identifying peaks (at 20.4°, 35.7° and 51.4° attributed to the (001), (110), (200) facets of LiOH) increased, the process is much slower than that on MWNTs cathode from cell with pristine Li. The presence of LiOH on both cathode and anode indicates the irreversible consumption of Li. The application of coating layer effectively reduces the Li loss that normally arose from the dendritic growth, volume change and corrosion during stripping/plating process, which subsequently reduces the polarization and alleviates the cathode passivation.

Further investigation using electrochemical impedance proves the protection effect of the artificial layer. After cycling for 58 times, N_2 was introduced into LOBs to remove O_2 for 30 min,

and then the resistance of LOBs was characterized using EIS. Figure S11 presents the Nyquist plots of the LOBs with pristine Li, Li-GO, Li-SiO_2 and Li-SiO_2/GO as anodes, and the equivalent circuit. Solution resistance (R_s), constant phase element 1 (CPE_1) and charge transfer resistance (R_1) at high frequency region are assigned to the impedance at the Li/electrolyte interface, constant phase element (CPE_2) and charge transfer resistance (R_2) at medium frequency region are contributed to the impedance at the solid products/cathode interface. Values of resistance are showed in Table S2. The R_s, R_1, and R_2 of Li-O_2 battery with pure Li are 219.0, 248.5 and 329.0 Ω, respectively. Those values of cell anode coated with GO and SiO_2 layers are reduced to 48.4, 83.4, 93.4 Ω, and 41.4, 69.3, 86.4 Ω, respectively. The values are further reduced to 34.2, 17.8 and 74.1 Ω with Li-SiO_2/GO coated anode. In agreement with morphology observation in Figure 6 and Figure 7, EIS results confirmed that the protection coatings led to more stable Li anode and less passivated cathode.

We considered that the nano/mesopores introduced by SiO_2 NPs in the coating layer not only facilitate the diffusion of Li ions, but also serve to guide the uniform Li ion flux in the stripping/plating process, which reduces the risk of localized Li dissolution and suppresses the dendritic growth of Li.[53-58] In practical LOBs, the introduction of oxygen reduction reaction (ORR) brings soluble intermediates (like O_2^- and LiO_2^- etc.) and the decomposed by-products of electrolyte.[40,58] These may immigrate through the glass fiber separator and cause serious chemical corrosion of Li anodes. Here, the incorporation of SiO_2 and GO manifests a synergistic effect of barrier effect, the ionic conductance and Li ion flux guidance. The SiO_2/GO layer in this research provides the best protection for Li anode, leading to the most stable LOB that has never been reported elsewhere.

CONCLUSIONS

In summary, we describe a facile strategy to preserve Li anode by coating a SiO_2/GO composite layer, so that the dendritic growth and chemical corrosion of Li Anode during the electro-chemical activities can be largely minimized or prevented. The structural composite layer with a large amount of nanopores resulted from the intercalation of SiO_2 NPs among the GO sheets, yield an enhanced transportation of Li ion. The resulted LOB with Li-SiO_2/GO anode can reach more than 348 cycles at 1 $A{\cdot}g^{-1}$ with a capacity of 1000 $mAh{\cdot}g^{-1}$, several folds of those cells with the pristine Li (58 cycles), Li-GO (166 cycles) and Li-SiO_2 (187 cycles) anodes. The rate performance and ultimate capacity of the LOB with Li-SiO_2/GO anode are also significantly improved. We hope this low-cost coating strategy find applications in future Li-ion batteries technologies.

ASSOCIATED CONTENT

Supporting Information.

The Supporting Information is available free of charge at https://

TEM images, ultimate capacities curves of LOBs, cyclic performance comparison of LOBs, SEM images, XRD patterns, and Nyquist plots and table of LOBs EIS analysis (PDF)

AUTHOR INFORMATION

Corresponding Author

Kun Luo - *School of Materials Science and Engineering, Changzhou University, Changzhou 213164, P. R. China; Email:luokun@cczu.edu.cn.*

Xiaoteng Liu - *Department of Mechanical & Construction Engineering, Faculty of Engineering and Environment, Northumbria University, Newcastle upon Tyne, NE1 8ST, UK; Email:terence.liu@northumbria.ac.uk.*

Present Addresses

Zhihong Luo - *College of Materials Science and Engineering, Guilin University of Technology, Guilin 541004, P. R. China*

Guangbin Zhu - *College of Materials Science and Engineering, Guilin University of Technology, Guilin 541004, P. R. China*

Liankun Yin - *College of Materials Science and Engineering, Guilin University of Technology, Guilin 541004, P. R. China*

Fujie Li - *College of Materials Science and Engineering, Guilin University of Technology, Guilin 541004, P. R. China*

Ben Bin Xu - *Department of Mechanical & Construction Engineering, Faculty of Engineering and Environment, Northumbria University, Newcastle upon Tyne, NE1 8ST, UK*

Laurent Dala - *Department of Mechanical & Construction Engineering, Faculty of Engineering and Environment, Northumbria University, Newcastle upon Tyne, NE1 8ST, UK*

Kun Luo - *College of Materials Science and Engineering, Guilin University of Technology, Guilin 541004, P. R. China*

Complete contact information is available at: https://

Author Contributions

The manuscript was written through contributions of all authors. All authors have given approval to the final version of the manuscript. ‡These authors contributed equally.

Notes

The authors declare no conflict of interest.

ACKNOWLEDGMENT

This work was supported by the National Natural Science Foundation of China (Grant No. 51874051), the UK Engineering Physics and Science Research Council (Grant No. EP/S032886/1) and Natural Science Foundation of Guangxi (Grant No. 2018GXNSFAA281184 and 2019GXNSFAA245046).

REFERENCES

(1) Feng, N. N.; He, P.; Zhou, H. S. Critical Challenges in Rechargeable Aprotic Li-O_2 Batteries. *Adv. Energy Mater.* **2016**, 6, 1502303.

(2) Yuan, T. Z.; Jiang, Y. Z.; Sun, W. P.; Xiang, B.; Lia, Y.; Yan, M.; Xu, B.; Dou, S. X. Ever-Increasing Pseudocapacitance in RGO-MnO-RGO Sandwich Nanostructure for Ultrahigh Rate Lithium Storage. *Adv. Funct. Mater.* **2016**, 26, 2198-2206.

(3) Jiang, Y. Z.; Li, Y.; Sun, W. P.; Huang, W.; Liu, J. B.; Xu, B.; Jin, C. H.; Ma, T. Y.; Wu, C. Z.; Yan, M. Spatially-Confined Lithiation/Delithiation in Highly Dense Nanocomposite Anodes Towards Advanced Lithium-Ion Batteries. *Energy Environ. Sci.* **2015**, 8, 1471-1479.

(4) Kong, L. P.; Liu, X. T.; Wei, J. J.; Wang, S.; Xu, B.; Long, D. H.; Chen, F. T-Nb_2O_5 Nanoparticle Enabled Pseudocapacitance with a Fast Li-Ion Intercalation. *Nanoscale* **2018**, 10, 14165-14170.

(5) Jiang, Y. Z.; Hu, M. J.; Zhang, D.; Yuan, T. Z.; Sun, W. P.; Xu, B.; Yan, M. Transition Metal Oxides for High Performance Sodium Ion Battery Anodes. *Nano Energy* **2014**, 5, 60-66.

(6) Yu, S. L.; Li, Y.; Lu, Y. H.; Xu, B.; Wang, Q. T.; Yan, M.; Jiang, Y. Z. A Promising Cathode Material of Sodium Iron-Nickel Hexacyanoferrate for Sodium Ion Batteries. *J. Power Sources* **2015**, 275, 45-49.

(7) Ma, S. C.; Zhang, Y. L.; Cui, Q. H.; Zhao, J.; Peng, Z. Q. Understanding Oxygen Reactions in Aprotic Li-O_2 Batteries. *Chin. Phys. B* **2016**, 25, 58-67.

(8) Guo, J. L.; Zhao, S. P.; Yang, H.; Zhang, F. X.; Liu, J. P. Electron Regulation Enabled Selective Lithium Deposition for Stable Anodes of Lithium-Metal Batteries. *J. Mater. Chem. A* **2019**, 7, 2184-2191.

(9) Cong, Y. G.; Geng, Z. B.; Sun, Y.; Yuan, L.; Wang, X. Y.; Zhang, X. B.; Wang, L.; Zhang, W.; Huang, K. K.; Feng, S. H. Cation Segregation of a-Site Deficiency Perovskite $La_{0.85}FeO_{3-\delta}$ Nanoparticles toward High-Performance Cathode Catalysts for Rechargeable Li-O_2 Battery. *ACS Appl. Mater. Interfaces* **2018**, 10, 25465-25472.

(10) Shu, C. Z.; Wu, C.; Long, J. P.; Guo, H. P.; Dou, S. X.; Wang, J. Z. Highly Reversible Li-O_2 Battery Induced by Modulating Local Electronic Structure via Synergistic Interfacial Interaction Between Ruthenium Nanoparticles and Hierarchically Porous Carbon. *Nano Energy* **2018**, 57, 166-175.

(11) Yu, H.; Dinh, K. N.; Sun, Y. M.; Fan, H. S.; Wang, Y. H.; Jing, Y.; Li, S. Z.; Srinivasan, M.; Yan, Q. Y. Performance-Improved Li-O_2 Batteries by Tailoring the Phases of Mo_xC Porous Nanorods as an Efficient Cathode. *Nanoscale* **2018**, 10, 14877-14884.

(12) Deng, H.; Qiao, Y.; Zhang, X. P.; Qiu, F. L.; Chang, Z.; He, P.; Zhou, H. S. Killing Two Birds with One Stone: a Cu Ion Redox Mediator for a Non-Aqueous Li-O_2 Battery. *J. Mater. Chem. A* **2019**, 7, 17261-17265.

(13) Kim, H.; Kwak, W. J.; Jung H. G.; Sun, Y. K. Verification for Trihalide Ions as Redox Mediators in Li-O_2 Batteries. *Energy Storage Mater.* **2019**, 19, 148-153.

(14) Dong, Q.; Yao, X. H.; Zhao, Y. Y.; Qi, M.; Zhang, X. Z.; Sun, H. Y.; He, Y. M.; Wang, D. W. Cathodically Stable Li-O_2 Battery Operations Using Water-in-Salt Electrolyte. *Chem.* **2018**, 4, 1345-1358.

(15) Assary, R. S.; Lu, J.; Du, P.; Luo, X. Y.; Zhang, X. Y.; Ren, Y.; Curtiss, L. A.; Amine, K. The Effect of Oxygen Crossover on the Anode of a Li-O_2 Battery Using an Ether-Based Solvent: Insights from Experimental and Computational Studies. *ChemSusChem* **2013**, 6, 51-55.

(16) Lin, D. C.; Liu, Y. Y.; Cui, Y. Reviving the Lithium Metal Anode for High-Energy Batteries. *Nat. Technol.* **2017**, 12, 194-206.

(17) Guo, Z. Y.; Wang, F. M.; Li, Z. J.; Yang, Y.; Tamirat, A. G.; Qi, H. C.; Han, J. S.; Li, W.; Wang, L.; Feng, S. H. Lithiophilic Co/Co_4N Nanoparticles Embedded in Hollow N-Doped Carbon Nanocubes Stabilizing Lithium Metal Anodes for Li-Air Batteries. *J. Mater. Chem. A* **2018**, 6, 22096-22105.

(18) Kim, B. G.; Kim, J. S.; Min, J.; Lee, Y. H.; Choi, J. H.; Jang, M. C.; Freunberger, S. A.; Choi, J. W. A Moisture- and Oxygen-Impermeable Separator for Aprotic Li-O_2 Batteries. *Adv. Funct. Mater.* **2016**, 26, 1747-1756.

(19) Xin, X.; Ito, K.; Dutta A.; Kubo, Y. Dendrite-Free Epitaxial Growth of Lithium Metal during Charging in Li-O_2 Batteries. *Angew. Chem. Int. Ed.* **2018**, 57, 13206-13210.

(20) Song, H. C.; Deng, H.; Li, C.; Feng, N. N.; He, P.; Zhou, H. S. Advances in Lithium-Containing Anodes of Aprotic Li-O_2 Batteries: Challenges and Strategies for Improvements. *Small Methods* **2017**, 1, 1700135.

(21) Zhang, P.; Zhao, Y.; Zhang, X. B. Functional and Stability Orientation Synthesis of Materials and Structures in Aprotic Li-O_2 Batteries. *Chem. Soc. Rev.* **2018**, 47, 2921-3004.

(22) Yin, Y. B.; Yang, X. Y.; Chang, Z. W.; Zhu, Y. H.; Liu, T.; Yan, J. M.; Jiang, Q. A Water-/Fire Proof Flexible Lithium-Oxygen Battery Achieved by Synergy of Novel Architecture and Multifunctional Separator. *Adv. Mater.* **2018**, 30, 1703791.

(23) Luo, K.; Zhu, G. B.; Zhao, Y. Z.; Luo, Z. H.; Liu, X. T.; Zhang, K.; Li, Y. L.; Scott, K. Enhanced Cycling Stability of Li-O_2 Batteries by Using a Polyurethane/SiO_2/Glass Fiber Nanocomposite Separator. *J. Mater. Chem. A* **2018**, 6, 7770-7776.

(24) Xu, J. J.; Liu, Q. C.; Yu, Y.; Wang, J.; Yan, J. M.; Zhang, X. B. In Situ Construction of Stable Tissue-Directed/Reinforced Bifunctional Separator/Protection Film on Lithium Anode for Lithium-Oxygen Batteries. *Adv. Mater.* **2017**, 29, 1606552.

(25) Koch, S. L.; Morgan, B. J.; Passerini, S.; Teobaldi, G. Density Functional Theory Screening of Gas-Treatment Strategies for Stabilization of High Energy-Density Lithium Metal Anodes. *J. Power Sources* **2015**, 296, 150-161.

(26) Liu, Q. C.; Xu, J. J.; Yuan, S.; Chang, Z. W.; Xu, D.; Yin, Y. B.; Li, L.; Zhong, H. X.; Jiang, Y. S.; Yan, J. M.; Zhang, X. B. Artificial Protection Film on Lithium Metal Anode toward Long-Cycle Life Lithium-Oxygen Batteries. *Adv. Mater.* **2015**, 27, 5241-5247.

(27) Yoo, E.; Zhou, H. S. Enhanced Cycle Stability of Rechargeable Li-O_2 Batteries by the Synergy Effect of a LiF Protective Layer on the Li and DMTFA Additive. *ACS Appl. Mater. Interfaces* **2017**, 9, 21307-21313.

(28) Asadi, M.; Sayahpour, B.; Abbasi, P.; Ngo, A. T.; Karis, K.; Jokisaari, J. R.; Liu, C.; Narayanan, B.; Gerard, M.; Yasaei, P.; Hu, X.; Mmukherjee, A.; Lau, K. C.; Assary, R. S.; Khalili-Araghi, F.; Klie, R. F.; Curtiss, L. A.; Salehi-Khojin, A. A Lithium-Oxygen Battery with a Long Cycle Life in an Air-Like Atmosphere. *Nature* **2018**, 55, 502-506.

(29) Huang, Z. M.; Ren, J.; Zhang, W.; Xie, M. L.; Li, Y. K.; Sun, D.; Shen Y.; Huang, Y. H. Protecting the Li-Metal Anode in a Li-O_2 Battery by Using Boric Acid as an SEI-Forming Additive. *Adv. Mater.* **2018**, 30, 1803270.

(30) Tang, W.; Yin, X.; Chen, Z.; Fu, W.; Loh, K. P.; Zheng, G. W. Chemically Polished Lithium Metal Anode for High Energy Lithium Metal Batteries. *Energy Storage Mater.* **2018**, 14, 289-296.

(31) Luo, Z. H.; Zhu, G. B.; Guo, L. L.; Li, F. J.; Li, Y. B.; Fu, M.; Cao, Y. C.; Li, Y. L.; Luo, K. Improving Cyclability and Capacity of Li-O_2 Batteries via Low Rate Pre-Activation. *Chem. Commun.* **2019**, 55, 2094-2097.

(32) Sun, Z.; Wang, H. R.; Wang J.; Zhang, T. Oxygen-Free Cell Formation Process Obtaining LiF Protected Electrodes for Improved Stability in Lithium-Oxygen Batteries. *Energy Storage Mater.* **2019**, 23, 670-677.

(33) Zhang, X.; Zhang, Q. M.; Wang, X. G.; Wang, C. Y.; Chen, Y. N.; Xie, Z. J.; Zhou, Z. An Extremely Simple Method for Protecting Lithium Anodes in Li-O_2 Batteries. *Angew. Chem. Int. Ed.* **2018**, 57, 12814-12818.

(34) Liao, K. M.; Wu, S. C.; Mu, X. W.; Lu, Q.; Han, M.; He, P.; Shao, Z. P.; Zhou, H. S. Developing a "Water-Defendable" and "Dendrite-Free" Lithium-Metal Anode Using a Simple and Promising $GeCl_4$ Pretreatment Method. *Adv. Mater.* **2018**, 30, 1705711.

(35) Zhang, T.; Liao, K. M.; He, P.; Zhou, H. S. A Self-Defense Redox Mediator for Efficient Lithium-O_2 Batteries. *Energy Environ. Sci.* **2016**, 9, 1024-1030.

555 (36) Zhao, X. H.; Sun, Z.; Yao, Z. G.; Cui, Z. H.; Wang, J. C.; Zhang, T. Halosilane Triggers
556 Anodic Silanization and Cathodic Redox for Stable and Efficient Lithium-O_2 Batteries. *J. Mater.*
557 *Chem. A* **2019**, 7, 18237-18243.
558 (37) Lee, D. J.; Lee, H. K.; Song, J. C.; Ryou, M. H.; Lee, Y. M.; Kim, H. T.; Park, J. K.
559 Composite Protective Layer for Li Metal Anode in High-Performance Lithium-Oxygen Batteries.
560 *Electrochem. Commun.* **2014**, 40, 45-48.
561 (38) Kim, J. H.; Woo, H. S.; Kim, W. K.; Ryu, K. H.; Kim, D. W. Improved Cycling Performance
562 of Lithium-Oxygen Cells by use of a Lithium Electrode Protected with Conductive Polymer and
563 Aluminum Fluoride. *ACS Appl. Mater. Interfaces* **2016**, 8, 32300-32306.
564 (39) Li, N.; Zhang, K.; Xie, K. Y.; Wei, W. F.; Gao, Y.; Bai, M. H.; Gao, Y. L.; Hou, Q.; Shen,
565 C.; Xia, Z. H; Wei, B. Q. Reduced-Graphene-Oxide-Guided Directional Growth of Planar Lithium
566 Layers. *Adv. Mater*. **2019**, 32,1907079.
567 (40) Kim J. S.; Kim D. W.; Jung H. T.; Choi J. W. Controlled Lithium Dendrite Growth by a
568 Synergistic Effect of Multilayered Graphene Coating and an Electrolyte Additive , *Chem. Mater*.
569 **2015**, 27, 2780-2787.
570 (41) Zhao, J.; Zhou, G. M.; Yan, K.; Xie, J.; Li, Y. Z.; Liao, L.; Jin, Y.; Liu, K.; Hsu, P. C.; Wang,
571 J. Y.; Cheng, H. M.; Cui, Y. Air-Stable and Freestanding Lithium Alloy/Graphene Foil as an
572 Alternative to Lithium Metal Anodes. *Nat. Nanotechnol*. **2017**, 12, 993-999.
573 (42) Shen, X. W.; Li, Y. T.; Qian, T.; Liu, J.; Zhou, J. Q.; Yan, C. L.; Goodenough, J. B. Lithium
574 Anode Stable in Air for Low-Cost Fabrication of a Dendrite-Free Lithium Battery. *Nat. Commun.*
575 **2019**, 10, 900.
576 (43) Gao, Y.; Yan, Z. F.; Gray, J. L.; He, X., Wang, D. W.; Chen, T. H.; Huang, Q. Q.; Li, Y. C.;
577 Wang, H. Y.; Kim, S. H.; Mallouk, T. E.; Wang, D. H. Polymer-Inorganic Solid-Electrolyte

578 Interphase for Stable Lithium Metal Batteries under Lean Electrolyte Conditions. *Nat. Mater.* **2019**,
579 18, 384-389.
580 (44) Tang, S.; Lan, Q.; Xu, L.; Liang, J. Y.; Lou, P.; Liu, C.; Mai, L. Q.; Cao, Y. C.; Cheng, S. J.
581 A Novel Cross-Linked Nanocomposite Solid-State Electrolyte with Super Flexibility and
582 Performance for Lithium Metal Battery. *Nano Energy*, **2020**, 10.1016/j.nanoen.2020.104600.
583 (45) Lin, D. C.; Yuen, P. Y.; Liu, Y. Y.; Liu, W.; Liu, N.; Dauskardt, R. H.; Cui, Y. A Silica-
584 Aerogel-Reinforced Composite Polymer Electrolyte with High Ionic Conductivity and High
585 Modulus. *Adv. Mater*. **2018**, 30, 1802661.
586 (46) Luo, Z. H.; Zhu, L. H.; Zhang, H. Y.; Tang, H. Q. Polyaniline Uniformly Coated on
587 Graphene Oxide Sheets as Supercapacitor Material with Improved Capacitive Properties. *Mater.*
588 *Chem. Phys.* **2013**, 139, 572-579.
589 (47) Xu, J. J.; Wang, K.; Ze, S. Z.; Han, B. H.; Wei, Z. X. Hierarchical Nanocomposites of
590 Polyaniline Nanowire Arrays on Graphene Oxide Sheets with Synergistic Effect for Energy
591 Storage. *ACS Nano* **2010**, 4, 5019-5026.
592 (48) Liu, S.; Deng, L. J.; Guo, W. Q.; Zhang, C. Y.; Liu, X. J.; Luo, J. Y. Bulk Nanostructured
593 Materials Design for Fracture-Resistant Lithium Metal Anodes. *Adv. Mater.* **2019**, 31, 1807585.
594 (49) Cheng, X. B.; Yan, C.; Peng, H. J.; Huang, J. Q.; Yang, S. T.; Zhang, Q. Sulfurized Solid
595 Electrolyte Interphases with a Rapid Li^+ Diffusion on Dendrite-Free Li Metal Anodes. *Energy*
596 *Storage Mater.* **2018**, 10, 199-205.
597 (50) Pan, R. J.; Sun, R.; Wang, Z. H.; Edström, K.; Strømme, M.; Nyholm, L. Sandwich-
598 Structured Nano/Micro Fiber-Based Separators for Lithium Metal Batteries. *Nano Energy* **2019**,
599 55, 316-326.

(51) Ye, H.; Zheng, Z. J.; Yao, H. R. Guiding Uniform Li Plating/Stripping via Lithium Aluminum Alloying Medium for Long-Life Li Metal Batteries. *Angew. Chem. Int. Ed.* **2019**, 58, 1094-1099.

(52) Sun, F.; Gao, R.; Zhou, D.; Osenberg, M.; Dong, K.; Kardjilov, N.; Hilger, A.; Markötter, H.; Bieker, P. M.; Liu, X. F.; Manke, I. Revealing Hidden Facts of Li Anode in Cycled Lithium-Oxygen Batteries through X-Ray and Neutron Tomography. *ACS Energy Lett.* **2019**, 4, 306-316.

(53) Bai, S. Y.; Sun, Y.; Yi, J.; He, Y. B.; Qiao Y.; Zhou, H. S. High-Power Li-Metal Anode Enabled by Metal-Organic Framework Modified Electrolyte. *Joule* **2018**, 2, 2117-2132.

(54) Zhang, R.; Chen, X.; Shen, X.; Zhang, X. Q.; Chen, X. R.; Cheng, X. B.; Yan, C.; Zhao, C. Z.; Zhang, Q. Coralloid Carbon Fiber-Based Composite Lithium Anode for Robust Lithium Metal Batteries. *Joule* **2018**, 2, 764-777.

(55) Zhang, H. M.; Liao, X. B.; Guan, Y. P.; Xiang, Y.; Li, M.; Zhang, W. F.; Zhu, X. Y.; Ming, H.; Lu, L.; Qiu, J. Y.; Huang, Y. Q.; Cao, G. P.; Yang, Y. S.; Mai, L. Q.; Zhao, Y.; Zhang, H. Lithiophilic-Lithiophobic Gradient Interfacial Layer for a Highly Stable Lithium Metal Anode. *Nat. Commun.* **2018**, 9, 3729.

(56) Liu, Y. Y.; Xiong, S. Z.; Wang, J. L.; Jiao, X. X.; Li, S.; Zhang, C. F.; Song, Z. X.; Song, J. X. Dendrite-Free Lithium Metal Anode Enabled by Separator Engineering via Uniform Loading of Lithiophilic Nucleation Sites. *Energy Storage Mater.* **2019**, 19, 24-30.

(57) Wang, X.; Wang, B.; Tang, Y.; Xu, B.B.; Liang, C.; Yan, M.; Jiang, Y.Z. Manganese Hexacyanoferrate Reinforced by PEDOT Coating Towards High-rate and Long-life Sodium-ion Battery Cathode. *J. Mater. Chem. A* **2020**, 6, 3222-3227.

(58) Kwak, W. J.; Park, J.; Nguyen, T. T.; Kim, H.; Byon, H. R.; Jang, M.; Sun, Y. K. A Dendrite- and Oxygen-Proof Protective Layer for Lithium Metal in Lithium-Oxygen Battery. *J. Mater. Chem. A* **2019**, 7, 3857-3862.

Figure captions

Figure 1 (a) TEM image of the SiO_2/GO hybrid; (b) N_2 adsorption/desorption isotherms; (c) pore distribution in the GO, SiO_2 and SiO_2/GO coatings; (d) XRD analysis of the GO, SiO_2 and SiO_2/GO coatings. Surface (e, f, g, h) and cross-section (i, j, k, l) images: (e, i) the pristine Li, (f, j) Li-GO, (e, k) Li-SiO_2 and (h, l) Li-SiO_2/GO anodes.

Figure 2 (a) Nyquist plots of the Li|SS cells with the pristine Li, Li-GO, Li-SiO_2 and Li-SiO_2/GO anodes and (b) the enlarged view of the green dotted frame, (c) ionic conductivity and (d) electron conductivity of GO, SiO_2 and SiO_2/GO coatings.

Figure 3 (a) Li stripping/plating curves in Li|Li symmetric cells with pristine Li, Li-GO, Li-SiO_2 and Li-SiO_2/GO at 0.1 $mA \cdot cm^{-2}$. The selected voltage profiles in the ranges from (b) 0 h to 4 h, (c) 132 h to136 h, (d) 408 h to 412 h, and (e) 614 h to 618 h. Surface morphology and cross-section images of (f, j) Li, (g, k) Li-GO after 200 h, (h, l) Li-SiO_2 and (i, m) Li-SiO_2/GO after 800 h

Figure 4 Cyclic stability (a, b, c, d) and rate performance (e, f, g, h) of the LOBs with: (a, e) the pristine Li, (b, f) Li-GO, (c, g) Li-SiO_2 and (d, h) Li-SiO_2/GO anodes.

Figure 5 C_{1s}, Li_{1s} and O_{1s} spectrum for SEI components of pristine Li anode (top) and after 10 cycles (bottom): (a) Li anode, (b) Li-GO anode, (c) Li-SiO_2 anode and (d) Li-SiO_2/GO anode.

Figure 6 Surface of Li anode at the 58th cycle: (a) pristine Li, (b) Li-GO anode, (c) Li-SiO_2 anode and (d) Li-SiO_2/GO anode; cross-section of (i) the pristine Li and Li anode at the 58th cycle: (f) Li-GO anode, (g) Li-SiO_2 anode, and (h) Li-SiO_2/GO anode, XRD patterns of Li anode at the 58th cycle: (i) pristine Li anode, (j) Li-GO anode, (k) Li-SiO_2 anode, and (l) Li-SiO_2/GO anode.

Figure 7 SEM images of (a) the pristine MWNTs cathode and (b) the MWNTs cathode in the LOBs with the Li anode at the 58th cycle, (c and f) the Li-GO anode at the 58th and 166th cycles, (d and g) the Li-SiO_2 anode at the 58th and 187th cycles, (e and h) the Li-SiO_2/GO anode at the 58th and 348th cycles.

Figure. 1

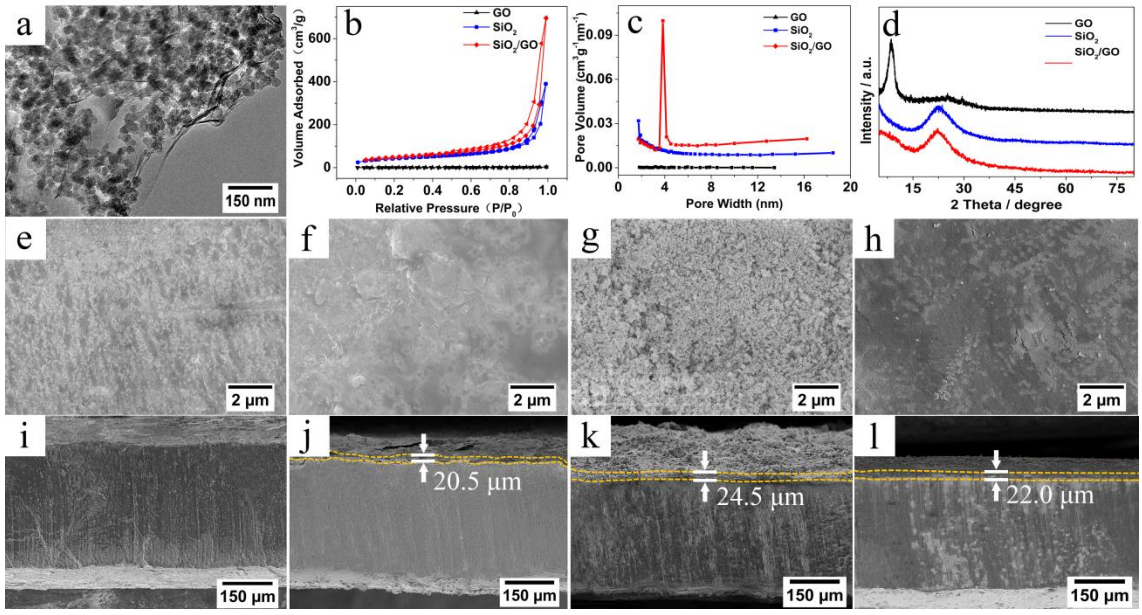

661

662

663 **Figure. 2**

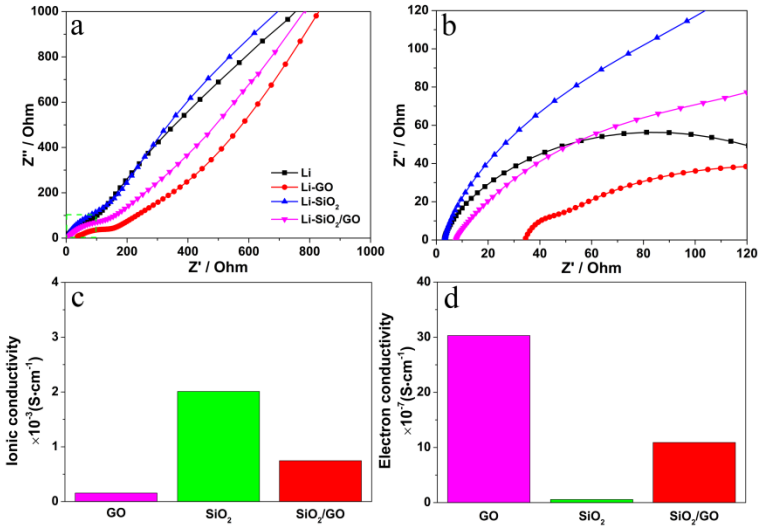

664

665

666

667 **Figure. 3**

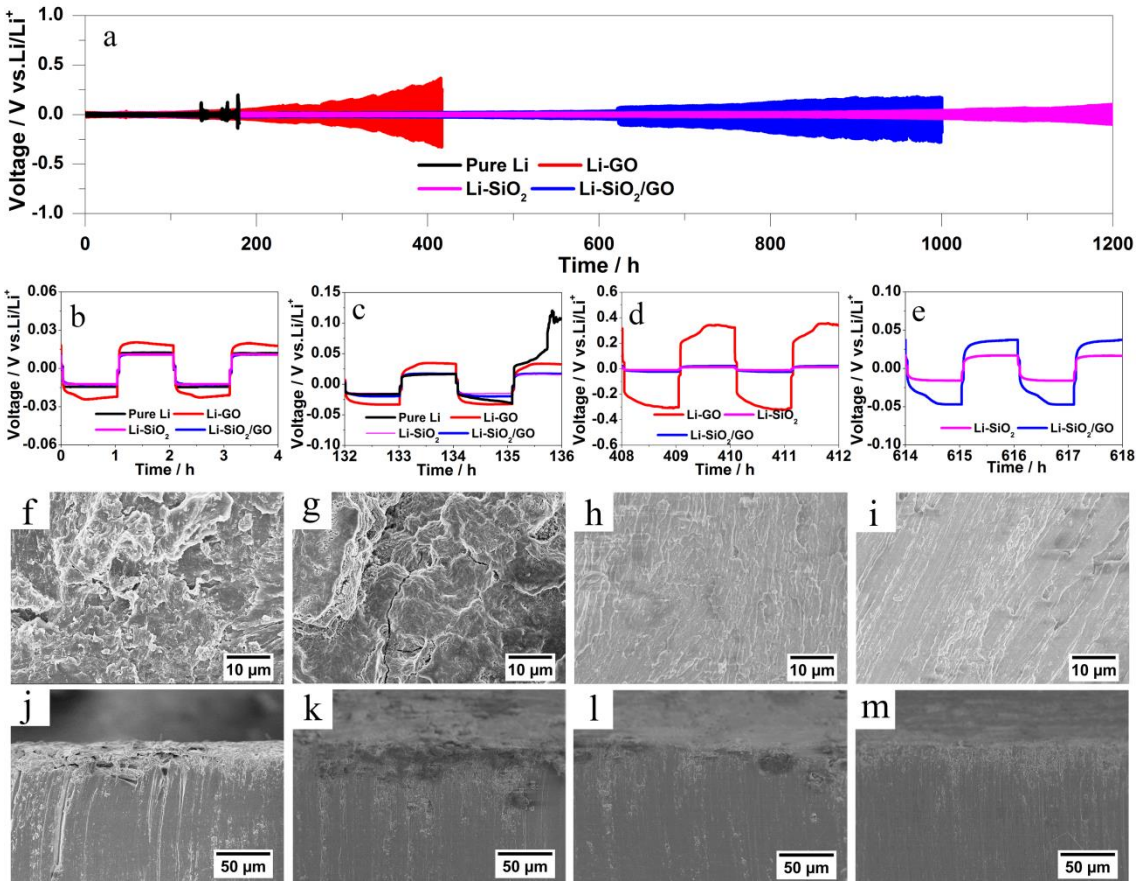

668

669

670

671

672

673

674

675 **Figure. 4**

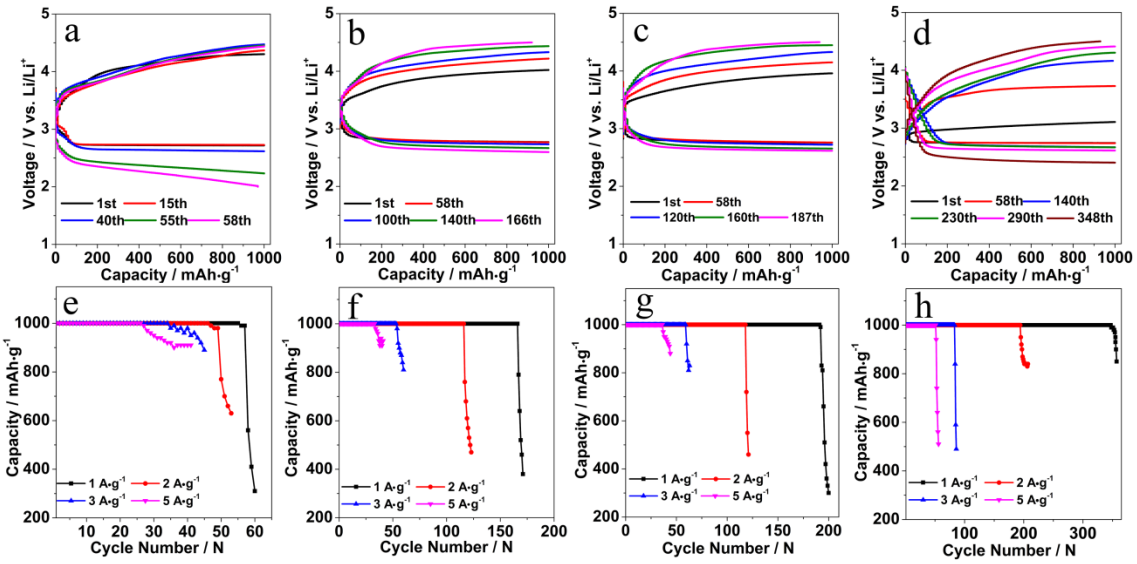

676

677 **Figure. 5**

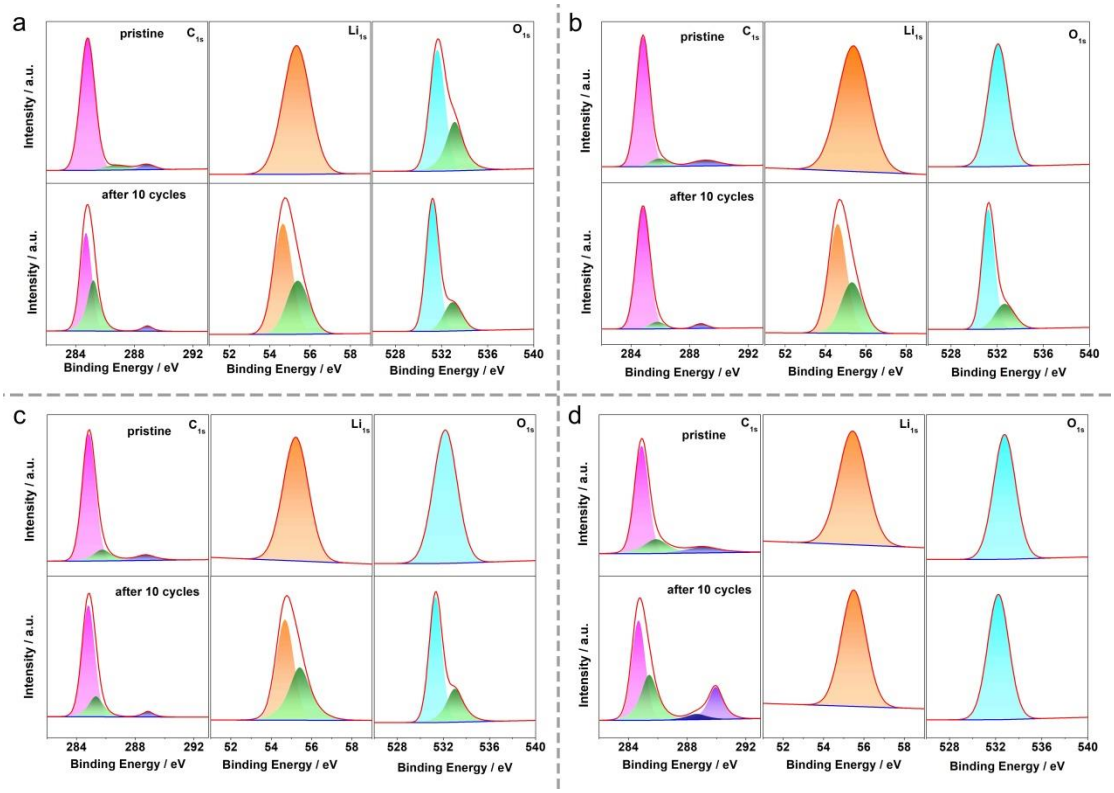

678

679

680 **Figure. 6**

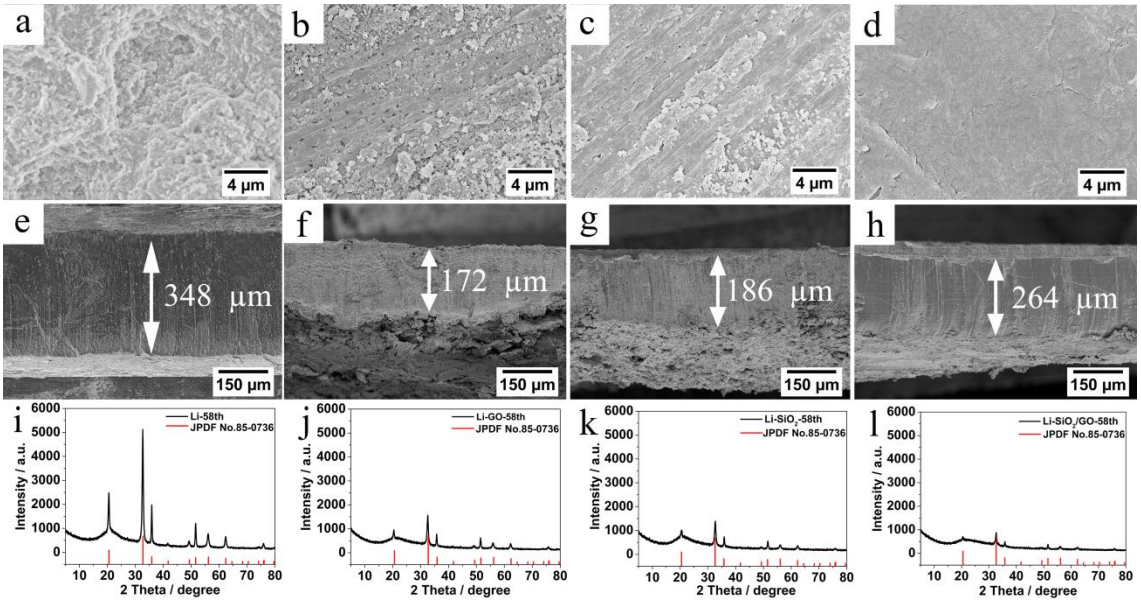

681

682

683 **Figure. 7**

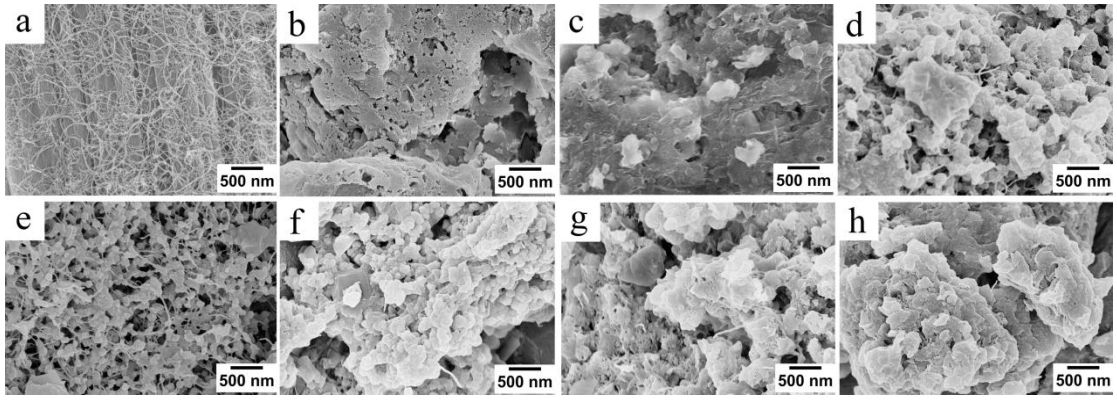

684

685

686

687